SLAC-PUB-13136

High harmonic generation for N_2 and CO_2 beyond the two-point model

M Gühr[1,2], B K McFarland[1,2], J P Farrell[1,2] and P H Bucksbaum[1,2]

[1] Stanford PULSE Center, Physics Department, Stanford University, CA 94305, USA
[2] Stanford Linear Accelerator Center, Menlo Park, CA 94025, USA

E-mail: mguehr@stanford.edu

Received 12 July 2007, in final form 2 August 2007
Published 7 September 2007
Online at stacks.iop.org/JPhysB/40/3745

Abstract
Strong field high harmonic generation (HHG) can reveal the quantum structure of the source molecule. We calculate the effect of interference between the recombining photoelectron and the orbital from which it was field ionized in the single-active-electron standard picture of HHG in N_2 and CO_2. We compare our results for the highest occupied molecular orbitals (HOMO's) to the predictions of a popular two-point scattering model. For N_2, we find an agreement for very large internuclear separations and no agreement for the ground-state internuclear distance. We reduce the arguments to the Fourier transform of the HOMO, which depends on the internuclear separation. For CO_2, we distinguish between two geometries. For one of these, we find a perfect agreement with the two-point scattering model; however, the emitted radiation is not phase matched in this case. The experimentally accessible radiation does not agree with the simple model.

1. Introduction

The generation of high harmonics from an ultrafast laser pulse has attracted attention for VUV and soft x-ray generation [1, 2] and the generation of attosecond pulses [3, 4]. Moreover, it has been shown that high harmonic generation (HHG) on molecules can be used to image molecular orbitals [5], using amplitude and phase information from the high harmonics within the framework of the three-step model [6, 7]. A plane electron wave containing different kinetic energies is superimposed with the HOMO from which it was initially ionized. The superposition gives rise to constructive and destructive interferences in the emitted high harmonics (HH). The two-point scattering model of Lein *et al* (sometimes referred to as two-centre interference model) interprets the interferences based on the internuclear separation R and the angle θ between the internuclear axis and the recolliding electron wave vector [8–11].

Submitted to J.Phys.B

Work supported in part by US Department of Energy contract DE-AC02-76SF00515

The superposition of an electron with de Broglie wavelength λ_{dB} with the molecular HOMO will give rise to interference that is constructive for

$$R\cos\theta = \left(n - \frac{1}{2}\right)\lambda_{\mathrm{dB}} \tag{1.1}$$

and destructive for

$$R\cos\theta = n\lambda_{\mathrm{dB}}, \tag{1.2}$$

if the molecular orbital has antibonding symmetry (e.g. CO_2 and O_2). For a bonding symmetry of the HOMO, the conditions are reversed [12]. Here n represents the order of the interference. The photon energy can be calculated from λ_{dB} and we comment on this below. Thus, the HH spectral maxima and minima can be translated into molecular parameters. Experimental molecular studies concentrate on N_2 [12, 13], having a HOMO σ_g symmetry or CO_2 [12–15] and O_2 [13] with a π_u symmetry. The two-point scattering model is used in [14, 15] to deduce the relation between λ_{dB} and the photon energy, referred to as the dispersion relation. It is still subject to a current debate [12, 14–16], since the experimental results on CO_2 from [12, 14] are contradictory. We check the applicability of the two-point scattering model in this paper for the N_2 and CO_2 HOMO's and find that in general it does not reproduce the interference features accurately. Combining the experimental results with our modelling will shed new light on the dispersion relation.

We calculate the interferences by a superposition of the free electron wave packet $\psi_{\mathrm{free}}(t)$ with the molecular HOMO ψ_{mol}. In order to model the wave packet's energy as a function of recollision time, we propagate the electrons classically in the laser electric field [6] without taking the Coulomb potential of the molecule into account. The maximal electron kinetic energy $E_{\mathrm{kin}}^{\mathrm{free}}$ at the point of recollision is given by $3.17U_p$, where the ponderomotive potential is $U_p = e^2E_{\mathrm{Laser}}^2/\left(4m_e\omega_{\mathrm{Laser}}^2\right)$ [6], with the electron mass m_e, its charge e, the laser field amplitude E_{Laser} and its optical frequency ω_{Laser}. The HH spectrum is given by the Fourier transform of the dipole acceleration. We calculate the HH spectrum of an atom or molecule by Fourier transforming the time-dependent dipole $\mathbf{d}(t)$, thereby neglecting the ω^4 term [16], where ω is the HH frequency. Since we are looking for modulations only, this is justified. The superposition $\psi(t) = \psi_{\mathrm{mol}}(t) + \psi_{\mathrm{free}}(t)$ forms an electric dipole $\langle\psi(t)|e\mathbf{r}|\psi(t)\rangle$ with the time-varying part:

$$\mathbf{d}(t) = \langle\psi_{\mathrm{mol}}(t)|e\mathbf{r}|\psi_{\mathrm{free}}(t)\rangle + c.c. \tag{1.3}$$

We refer to this model as the *time-dependent dipole model* throughout this paper. HHG is just the reverse process of VUV photoionization and $\langle\psi_{\mathrm{mol}}|e\mathbf{r}|\psi_{\mathrm{free}}(t)\rangle$ is the matrix element for VUV photoionization of the ground state, if the Coulomb potential is neglected. A periodic repetition of the ionization and recollision twice per period structures the emitted spectrum and leads to the exclusive emission of odd harmonics of the fundamental laser frequency (see, e.g. [3]).

In the case of pointlike atomic or molecular wavefunctions, the overlap of $\psi_{\mathrm{free}}(t)$ and ψ_{mol} according to equation (1.3) leads to a structureless spectral plateau extending to the cutoff. If, however, the molecular wavefunction has some structure, rich interference phenomena will be observed that lead to a modulation of the dipole formation in equation (1.3) and therefore to a modulation of the amplitude and phase of the emitted high harmonic light.

The spectral amplitude in the plateau region is found to be approximately constant in calculations [17] and is usually determined by a comparison to the experiment [5, 16]. To simplify our model we will assume that it is constant. The assumption has a negligible influence on the sharp interference minima that are the subject of this paper.

We will present two model cases for HHG on molecules. First we look at the change in the HHG spectrum as a function of the internuclear separation of N_2 and second we examine the dependence of the spectrum on the alignment angle in CO_2. We compare the latter results directly with the experimental information from [12, 14] and discuss the validity of the two-point scattering model. The discussion of the R variation in N_2 follows the tomographic imaging procedure used in [5].

2. Results

In order to calculate the time-dependent dipole matrix element in equation (1.3) we first need to calculate the system wavefunction ψ_{mol}, which is in our case the HOMO of N_2 or CO_2. Both are determined with the Gaussian 03 *ab initio* code [18] using the minimal basis set STO-3G. The free electron wavefunction $\psi_{\mathrm{free}}(t)$ is a plane wave $\psi_{\mathrm{free}}(t) = \exp(-\mathrm{i}k(t)x - \mathrm{i}\Phi(t))$, where $k(t) = \sqrt{2m_e E_{\mathrm{kin}}^{\mathrm{free}}(t)/\hbar^2}$ is the wave vector and $\Phi(t) = \int E_{\mathrm{kin}}^{\mathrm{free}}(t)/\hbar \, \mathrm{d}t$ is the temporal phase of the wave packet. The free electron kinetic energy $E_{\mathrm{kin}}^{\mathrm{free}}$ is determined by solving Newton's equations. We evaluate the interference conditions according to equation (1.3) and find the HH intensity as a function of λ_{dB}. Recent HHG analyses convert the de Broglie wavelength to a photon energy [16]. We will make the approximation that the electron is 'born' at the molecular centre of mass with zero kinetic energy, neglecting the molecular Coulomb potential. This underestimates the initial electron momentum by maximally $\sqrt{2I_p m_e}$. This error is smaller for electrons near the cutoff. A more serious difficulty is that $E_{\mathrm{kin}}^{\mathrm{free}}$ of the returning wave packet is evaluated at the molecular centre of mass, once more neglecting its Coulomb potential [19]. Since the free electron has to recombine with the HOMO, the emitted photon energy $\hbar\omega_p$ is given by the sum of the free electron kinetic energy plus the ionization potential $\hbar\omega_p = E_{\mathrm{kin}}^{\mathrm{free}} + I_p$. The energetic position of the calculated interference minima depends on $\lambda_{\mathrm{dB}} = h/\sqrt{2m_e E_{\mathrm{kin}}}$ of the recombining electron wave packet at the time of recollision and therefore only on the total kinetic energy E_{kin}. The actual value of the kinetic energy is given by $E_{\mathrm{kin}} = E_{\mathrm{kin}}^{\mathrm{free}} + \delta I_p$, where δI_p represents the portion of the molecular Coulomb potential which is converted into kinetic energy prior to recombination and δ varies between 0 and 1. The wave packet can maximally gain the total potential energy I_p ($\delta = 1$) as kinetic energy, so that $E_{\mathrm{kin}} = E_{\mathrm{kin}}^{\mathrm{free}} + I_p$. In that case, the interference features would be produced by $\lambda_{\mathrm{dB}} = h\big/\sqrt{2m_e\big(E_{\mathrm{kin}}^{\mathrm{free}} + I_p\big)}$. If the electron converts no potential energy to kinetic energy ($\delta = 0$), the relation $E_{\mathrm{kin}} = E_{\mathrm{kin}}^{\mathrm{free}}$ would hold. The interference feature appears in the photon spectrum at $\hbar\omega_p = E_{\mathrm{kin}}^{\mathrm{free}} + I_p = E_{\mathrm{kin}} - \delta I_p + I_p = h^2\big/\sqrt{2m_e\lambda_{\mathrm{dB}}^2} - \delta I_p + I_p$. For $\delta = 1$, we would not have to shift the interference minimum, and we could directly translate from a kinetic energy to a photon energy scale. In the latter case $\delta = 0$, the position of the interference minimum would be shifted up by I_p on the photon energy scale. In addition, the plane wave approximation neglects the focusing influence of the molecular Coulomb potential on the returning electron wave [5, 16, 17] and the effect of the Coulomb potential on the recollision time.

Figure 1(a) shows the HOMO of N_2 for two different internuclear separations $R = 3.5a_0$ and $R = 1.5a_0$. Clearly, the separations are very extreme, since the internuclear separation for the nitrogen ground state is $2a_0$. The free electron wave vector k_e is parallel to the internuclear axis. The time-dependent dipoles oscillate parallel to k_e. No perpendicular oscillation occurs for symmetry reasons. The Fourier transforms of the calculated dipoles according to equation (1.3) are shown in figures 1(b)–(e) as the solid lines. The dashed lines in the figures give the position of the destructive interference calculated with the two-point scattering model, using equation (1.1) with $n = 1$ for the bonding symmetry of the N_2 HOMO.

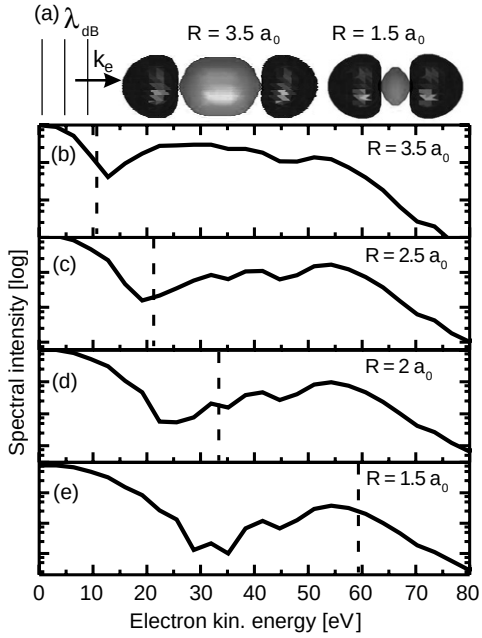

Figure 1. HHG from N_2 molecules with different internuclear separation R. (a) HOMO for N_2 in the STO-3G basis calculated with Gaussian for two different internuclear separations. The different grey shadings indicate opposite signs of the orbital. The recolliding electron wave with a wave vector k_e is indicated in the sketch. (b)–(e) Solid lines: Fourier transforms of the time-dependent dipoles parallel to k_e as calculated by equation (1.3). Spectral minima are clearly visible. The dashed lines mark the spectral minima as expected by the two-point scattering model equation (1.1), for bonding symmetry. For large internuclear separations, the minima from the calculated time-dependent dipole are overlapping with the minima predicted by the two-point scattering model. For short internuclear separations, significant discrepancies can be seen.

For the large internuclear distances $R = 3.5a_0$ and $R = 2.5a_0$ in figures 1(b) and (c), the minima from the time-dependent dipole calculation coincide with the minima predicted by the two-point scattering model. However, from $R = 2a_0$ to smaller internuclear distances, the minima suggested in the two-point model are shifted to higher energies with respect to the dipole calculation. For the ground-state equilibrium distance, the two-point scattering model predicts a minimum at 33 eV, whereas the dipole calculation leads to a minimum at 25 eV. For $R = 1.5a_0$, the discrepancy is even larger and is around 30 eV.

For the CO_2 molecule, we demonstrate the angle dependence of the HHG. The HOMO, having a π_g symmetry, is doubly degenerate. In contrast to nitrogen, the HOMO of CO_2 is antibonding. It consists of p lobes lying perpendicular to the internuclear axis and located at the oxygen atoms. The HHG calculations for CO_2 are divided into two different geometries. Geometry I is illustrated in figure 2(a). The internuclear axis and k_e define a plane, where k_e is the wave vector of the returning free electron wave packet $\psi_{\text{free}}(t)$. The orbital lobes are out of this plane in geometry I, whereas they lie in the plane for the degenerate orbital solution in geometry II. HHG from a linear combination of the two degenerate HOMO's can be decomposed into HHG from geometry I superimposed with the HHG from geometry II. The decomposition chosen here is convenient because it reflects a symmetry with respect to k_e. We evaluate the dipole oscillating in the direction perpendicular to k_e in (b)–(f), while the recombination angle θ is changed. Only dipole contributions oscillating perpendicular to k_e

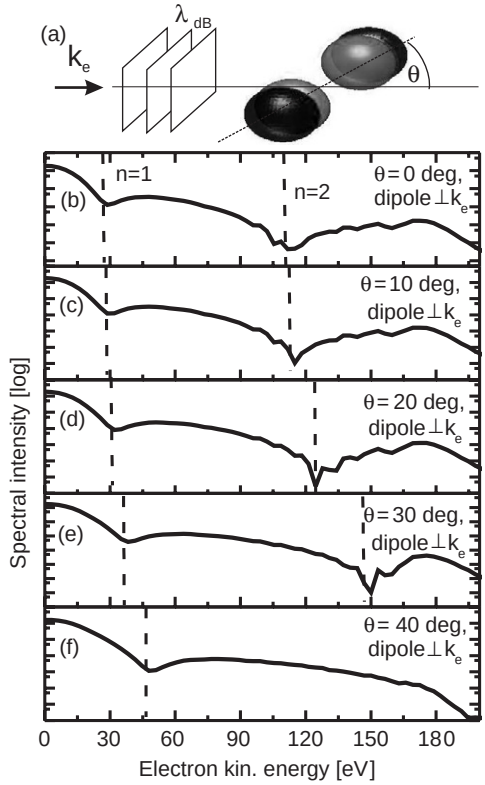

Figure 2. (a) Geometry I. HHG from CO_2 molecules with different recollision angles θ. The lobes of the π_g HOMO lie *out of the plane* defined by k_e and the internuclear axis. k_e is the wave vector of the recolliding free electron wave packet. (b)–(f) Solid lines: Fourier transforms of the time-dependent dipoles perpendicular to k_e as calculated by equation (1.3). Angle-dependent spectral minima are clearly visible. The dashed lines mark the spectral minima as expected by the two-point scattering model equation (1.2) for $n = 1, 2$ and antibonding symmetry, using $R = 2.32$ Å and the appropriate recollision angle θ.

are visible in the calculation. In the dipole approximation, the parallel contribution does not exist due to the HOMO symmetry. A dipole oscillating along k_e above the k_e-internuclear-axis plane is always cancelled by a π-phase-shifted dipole oscillating below the k_e-internuclear-axis plane. The Fourier-transformed perpendicular dipoles are shown in figures 2(b)–(f). As in the case of nitrogen, clear minima appear. Since we extended the cutoff over 200 eV by increasing the intensity to 9×10^{14} W cm^{-2}, an additional minimum at higher energies is visible corresponding to higher order interferences. The minima predicted by the two-point scattering model are marked by the dashed lines. For the antibonding symmetry, the form of equation (1.2) is used to describe the destructive interference by the two-point scattering model [12, 14, 15]. The electronic density is located at the oxygen atoms in the form of p-like orbitals. The equilibrium O–O distance is $4.4a_0$; we use this as R in our calculations with the two-point scattering model. The minima at low energies are calculated with $n = 1$. For the higher energies we used $n = 2$ in equation (1.2). For all recombination angles θ the prediction of the two-point scattering model fits well with the solid curves calculated with the time-varying dipole.

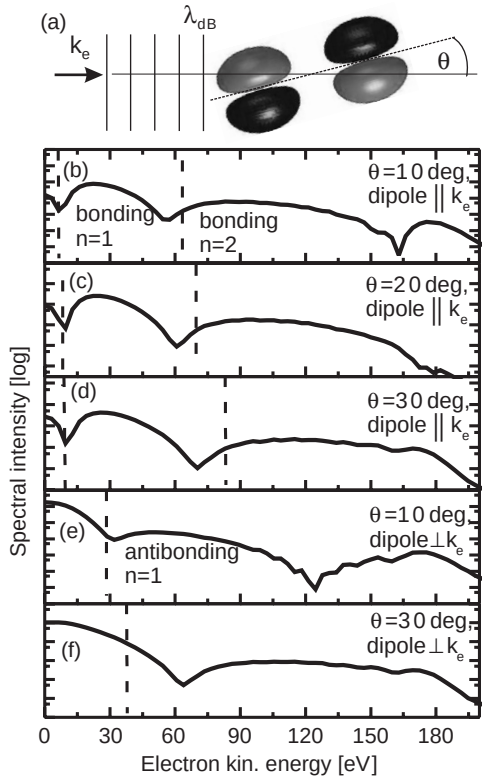

Figure 3. (a) Geometry II. HHG from CO_2 molecules with different recombination angles θ, the lobes of the π_g HOMO *in the plane* defined by k_e and the internuclear axis. (b)–(d) Solid curves: Fourier transforms of the time-dependent dipoles parallel to k_e as calculated by equation (1.3). Angle-dependent spectral minima are clearly visible. The dashed lines mark the spectral minima as expected by the two-point scattering model equation (1.1) for $n = 1$, 2 and *bonding* symmetry, using $R = 2.32$ Å and the appropriate recolliding angle θ. (e), (f) Solid curves: Fourier transforms of the time-dependent dipoles perpendicular to k_e as calculated by equation (1.3). The dashed lines mark the spectral minima as expected by the two-point scattering model equation (1.2) with $n = 1$ for *antibonding* symmetry.

Calculations for geometry II are presented in figure 3. In this particular geometry, the p lobes of the π_g HOMO lie in the plane defined by k_e and the internuclear axis. Taken together, geometries I and II thus describe a complete set of HHG symmetries. Any other orientation of the orbital with respect to k_e and the internuclear axis can be decomposed into the two geometries discussed here.

Figures 3(b)–(d) show the Fourier-transformed dipoles parallel to k_e as solid curves. Minima in the high harmonic spectrum are clearly visible. The dashed lines present the energetic positions of the minima calculated from the two-point scattering model, now however using equation (1.1), which represents the conditions for *bonding* symmetry. For $n = 1$ in equation (1.1) we observe a rather good agreement between the minima in the spectra and the modelled ones. For $n = 2$, the spectral minima always lie below the energy of the two-point scattering model predictions. Figures 3(e) and (f) show analog calculations for dipoles oscillating perpendicular to k_e for $\theta = 10^\circ$ and 30°. For comparison, we plot the two-point scattering minima for the antibonding symmetry as the dashed lines. For $\theta = 10^\circ$

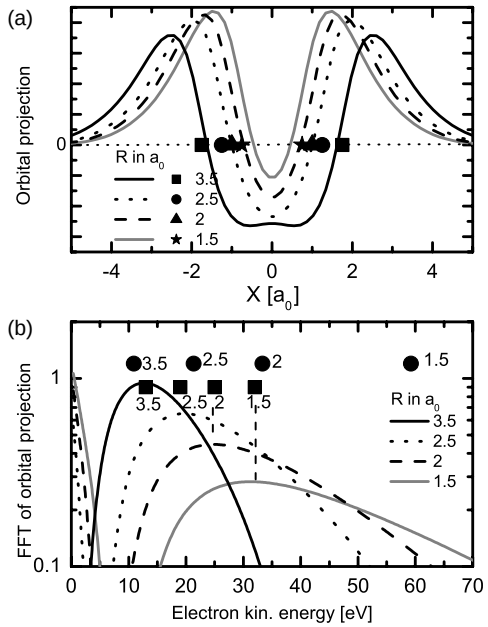

Figure 4. (a) Curves: the projections of N_2 HOMO orbitals on the internuclear axis for different R. Symbols denote the internuclear separations corresponding to the projections. (b) Curves: Fourier transform of the projections in (a). Symbols: the squares give the position of the minima from the curves in figures 1(b)–(e) where the respective internuclear separation is noted in a_0. The circles give the position of the destructive interference as calculated by the two-point scattering model according to equation (1.1).

we observe a good agreement; at 30° the two-point scattering model is lower in its prediction by 20 eV.

3. Discussion

For N_2 the spectral minima in the time-dependent dipole calculations clearly show a variation with the internuclear distance R. The spectral minima at internuclear distances larger than $2a_0$ coincide with the predictions of equation (1.1). Originally, the two-point scattering model was proposed to explain quantum simulations for HHG on H_2 and H_2^+. Equations (1.1) and (1.2) were used to explain constructive and destructive features, respectively. The N_2 two-point scattering model has already been discussed in [20]. However, the simple two-point scattering model according to formula (1.1) does not reflect the correct position for R equal and smaller than $2a_0$ (see figures 1(d) and (e)). The minima clearly depend on the shape of ψ_{mol}, which we assumed to be the HOMO for the purpose of our calculations using equation (1.3). To get further insight into the underlying physics, we projected the three-dimensional orbital structure of the N_2 HOMO onto the internuclear axis (see figure 4(a)). Since the recombining electron wave vector k_e is assumed to point towards the internuclear axis of N_2 and the σ_g orbital exhibits a cylindrical symmetry around this axis, the projection captures the main orbital features responsible for the HHG. While the internuclear distance is decreased from $3.5a_0$ to $1.5a_0$, the electronic structure of the HOMO shrinks. We performed a Fourier transformation of the projections to analyse the HOMO in momentum space. Using the free electron dispersion relation $E = p^2/2m$, we present the Fourier transforms as a function of the

electron kinetic energy in figure 4(b). The Fourier transform at $R = 3.5a_0$ has a peak around 10 eV, corresponding to the inverted distance of its orbital maxima in figure 4(a). Since the other HOMO's have their maxima shifted closer together in space, the corresponding maximum in the Fourier transform is shifted to higher energies. We compare the maxima of the HOMO projection's Fourier transform with the minima obtained from our time-dependent dipole calculations using equation (1.3). These are taken from the solid lines in figures 2(b)–(e) and are depicted in figure 4(b) as squares with the respective R in a_0. One finds that the position of the Fourier transform maxima corresponds very well to the minima from the time-dependent dipole model. For comparison, we also plot the prediction from equation (1.1) of the two-point scattering model as circles with respective internuclear separations R. As already seen in the context of figure 2, the minima overlap with the calculations and therefore with the HOMO Fourier transform maxima for large internuclear separations, but differ for those from $R = 2a_0$ and smaller.

The interference phenomena occur between the recombining plane wave $\psi_{\text{free}}(t)$ and an orbital ψ_{mol}. The interference can only modulate the spectrum, if the ψ_{mol} 'offers' a plane wave of the right wavelength for $\psi_{\text{free}}(t)$. That is essentially the idea of orbital tomography, which was successfully employed to image the N_2 HOMO [5]. The dash-dotted curve in figure 4(b), describing the FT of the N_2 HOMO at $R = 1.5a_0$, has a maximum at 33 eV. The two-point scattering model predicts a spectral minimum at about 60 eV, but since the Fourier amplitude is lowered by a factor of 2 with respect to the maximum, the spectral minimum will occur at 33 eV. The two-point scattering model overemphasizes the importance of R. The electron density of the HOMO is crucial and it is not necessarily connected to R. This argument was discussed in one of the first publications on the two-point scattering model by Lein and co-authors [9]. A derivation based on the very high localization of electron wavefunctions at the position of the nuclei is given there. This condition of [9] binds the electron density to the nuclear positions and therefore always predicts a Fourier transformation maximum at $2\pi/R$ in reciprocal space. The authors clearly discussed this non-realistic assumption and stated that the predictions of the model have to be carefully tested for more realistic diatomic HOMO's.

In real molecules, the charge density can be pushed away from nuclear positions if the orbitals are antisymmetric, as for example two s wavefunctions with opposite phase at the different nuclei or p-like lobes of opposite symmetry. The latter is true for the nitrogen molecule σ_g HOMO that is mainly set up from p lobes of opposite phase pointing along the internuclear axis, leading to the structure shown in figure 1(a). In fact, for small N_2 internuclear separations, we attribute the disagreement of the two-point scattering model with the time-dependent dipole minima to the pushed out charge density. For large internuclear distances, the p lobes do not overlap to a large extent and the charge density is symmetrically arranged around each nucleus. In the case of small internuclear distances R, the p lobes do overlap to a large extent and the charge density is antisymmetric around each nucleus. The antisymmetric superposition of p lobes pushes the charge density to larger separations. The positive maxima visible in figure 4(a) are pushed out to larger distances from the nuclei. This leads to a shift of the Fourier transform maxima to lower energies and longer de Broglie wavelengths. The situation gets more complicated due to the admixture of s orbitals. The *ab initio* calculation with Gaussian gives a coefficient of -0.068 for the 1s, 0.417 for the 2s and ± 0.6 for the 2p contribution, whereas the sign for the latter is different for the two nuclei. Zimmermann and co-authors discussed the influence of s–p mixing on the high harmonic spectrum [20], stating that this is responsible for a discrepancy between the two-point scattering model and the spectral minima obtained from their simulations. We have significant s contributions even for large internuclear distances of $2.5a_0$ and $3.5a_0$, where we observe a good agreement with

the two-point scattering model. At small internuclear separations, we still get a disagreement with the two-point scattering model if we take into account only the p contribution. This relates to the fact that the electron density is still pushed away from the nuclei in the p superposition.

We now discuss the angle-dependent HHG on CO_2 molecules. As figure 2 indicates, the two-point scattering model is in good agreement with the dipole simulations for all angles, assuming the p lobes to be pointing out of the k_e-internuclear-axis plane as in geometry I. The dipoles are oscillating perpendicular to the k_e vector. The minima shift to higher energies with increasing recombination angle θ. This is due to the fact that the distances between the p lobes in the k_e direction shrink as θ increases. Thus, the respective de Broglie wavelength for the interference has to be shorter. This, in turn, leads to an interference at higher electron energy. The two p lobes are far enough away from each other (the carbon atom is sitting between them) and have negligible spatial overlap. In addition, they do not posses any s admixture, which could complicate the interpretation according to [20]. Applying the interpretation of the N_2 results, we can state that the charge density of the p lobes is not deformed due to the overlap and that the internuclear distance is a good parameter to quantify the charge distribution. No dipole oscillation parallel to the k_e vector exists in geometry I, as explained above.

Geometry II has the p lobes in the k_e-internuclear-axis plane and gives rise to dipole oscillations parallel and perpendicular to k_e. Therefore, both dipoles are shown in figure 3. The Fourier transforms in figures 3(b)–(d) (dipole parallel to k_e) show two pronounced minima, both shifting to higher energies with increasing recombination angle θ, implying the same interpretation as in geometry I. However, the minima do not follow the two-point scattering model for *antibonding* orbitals, described by equation (1.2). Instead, we plotted the destructive two-centre predictions for a *bonding* symmetry (equation (1.2)) using the internuclear distance of CO_2. For $n = 1$, these predictions agree very well with the Fourier transforms of the dipole. For $n = 2$, the two-point scattering predictions systematically lie above the Fourier-transformed dipoles with increasing disagreement towards higher angles θ. We did not plot the $\theta = 0$ trace, since no dipole parallel to k_e is formed. The reason for the good agreement with the two-point scattering model for bonding orbitals is reflected in the sketch in figure 3(a). While travelling through the HOMO, the recolliding free electron wave packet experiences a structure with a symmetry similar to the N_2 HOMO at angles different from 0° and 90°. The reason for the deviation of the $n = 2$ minima is once more reflected by the discrepancy between electron orbital distances and nuclear distances, as in the case of N_2. The distance between the maxima of the dark grey phased lobes along the k_e direction is larger than the nuclear distance R. The predominant Fourier component of the orbital projection on the k_e direction then reflects a component with a longer de Broglie wavelength than predicted by the two-point scattering model.

In a real experiment, we are confronted with a mixture of recombination angles from both geometries I and II. A simplification is implemented experimentally by aligning the molecular ensemble by the interaction with a non-resonant laser pulse. If the laser pulse duration is shorter than the rotational period of the molecule, a coherent rotational wave packet is excited leading to rotational revivals with field-free alignment [21]. One can therefore create high harmonics on molecules with a narrow angular distribution without perturbing their levels by an alignment laser pulse.

Molecular alignment and phase matching [22] have a profound effect on HHG. The model calculations here only hold true for a single molecule at a definite angle. For example, dipoles oscillating in the direction of the laser propagation do not contribute to HHG, since they do not radiate in the forward direction. In an aligned ensemble, some of the dipoles oscillating perpendicular to k_e are not phase matched. Even more important, all perpendicular oscillating

dipoles cancel if the aligned ensemble has the internuclear axes arranged symmetrically around the polarization axis of the high harmonic generating laser. For each molecule that is off the polarization direction of the alignment pulse by a distinct angle θ, there is a mirror image having an inclination $-\theta$. Thus, a perpendicular dipole generated under the recombination angle θ has its counterpart at the angle $-\theta$ with equal strength but opposite sign. All perpendicular components will vanish in the phase matching process. This information is crucial, since the geometry I only gave rise to perpendicular dipoles. This was however the only direction in which we found an agreement with the two-point scattering model for the antibonding HOMO symmetry. In particular, it is important for the interpretation of the results of [12, 15]. Reference [14] makes use of the interference model to deduce the dispersion relation between k_e and the harmonic photons. The measurements were performed on an ensemble with cylindrical symmetry around the high harmonic generating laser polarization axis. Thus, only geometry II can account for the high harmonic emission. An experimental check for this is the measurement of the high harmonic polarization. No polarization perpendicular to the generating polarization should be visible in that case. Therefore, we can concentrate on the parallel dipoles presented in figures 3(b)–(d). The minima observed in the aligned ensemble depend crucially on the alignment parameters. The first-order minima are too low in energy to be observed in a real experiment. We plot our spectra as a function of the electron kinetic energy. As stated above the destructive interference appears in the 15.7 eV interval between the value given in figures 3(b)–(d) and this value plus I_p. The experimental results of [14] show a minimum at the 35th harmonic corresponding to a photon energy of 55 eV. At an angle θ of 10°, indeed a minimum at 55 eV is visible in the high harmonic spectra from phase-matched dipoles (figure 3(b)). This implies that the destructive interference as a function of high harmonic photon energy is unshifted with respect to the free electron kinetic energy. Thus, the total kinetic energy is given by the free electron kinetic energy plus the full Coulomb potential I_p. At angles bigger than 10°, the theoretical interval does not contain the experimental value anymore. If most of the molecules would lie at an angle of 10° with respect to the alignment polarization, our simulations would explain the experimental features, however using a different physical picture. Instead of deducing that the recombination process happens at the edge of the CO_2 HOMO [14, 15], we would argue that it happens when the electrons have gained the full I_p in their kinetic energy—meaning they recombine in the molecular potential well.

If the aligned ensemble is not cylindrically symmetric around the polarization of the high harmonic generating pulse, perpendicular dipole components will appear and the interpretation of the results is further complicated since geometries I and II mix and since the perpendicular components of geometry II set in.

Summarizing, we showed that the HHG spectra of N_2 and CO_2 showed minima due to interferences in the recombination of the free electron wave packet with the molecular HOMO. Our calculations using the time-dependent dipole picture show agreement with the two-centre model for large internuclear distances of N_2. For small internuclear distances a disagreement is found due to the shifted electronic density in the overlap of the two p lobes. For CO_2, we find an agreement with the two-centre model for geometry I, which has the p lobes in the plane that is defined by k_e and the internuclear axis. This geometry produces no high harmonic light if the aligned molecular distribution is cylindrically symmetric around the polarization of the high harmonic generating pulse. In geometry II, having the p lobes above and below the k_e-internuclear-axis plane, the two-centre model for antibonding symmetry is not valid. Instead we find the bonding symmetry predictions to lie close to the spectral minima for the radiated light. We can explain the results by Vozzi *et al* [14, 15] by our model assuming a recombination in the molecular potential well.

Acknowledgments

This paper was written at the Stanford PULSE Center, with support from the Stanford Linear Accelerator Center, a national laboratory operated by Stanford University on behalf of the US Department of Energy, Office of Basic Energy Sciences. MG thanks the Humboldt Foundation for financial support.

References

[1] L'Huillier A and Balcou P 1993 High-order harmonic generation in rare gases with a 1-ps 1053-nm laser *Phys. Rev. Lett.* **70** 774–7
[2] Macklin J J, Kmetec J D and Gordon C L 1993 High-order harmonic generation using intense femtosecond pulses *Phys. Rev. Lett.* **70** 766–9
[3] Baltuska A *et al* 2003 Attosecond control of electronic processes by intense light fields *Nature* **421** 611–5
[4] Kienberger R *et al* 2004 Atomic transient recorder *Nature* **427** 817–21
[5] Itatani J, Levesque J, Zeidler D, Niikura H, Pepin H, Kieffer J C, Corkum P B and Villeneuve D M 2004 Tomographic imaging of molecular orbitals *Nature* **432** 867–71
[6] Corkum P B 1993 Plasma perspective on strong field multiphoton ionization *Phys. Rev. Lett.* **71** 1994–7
[7] Kulander K C, Schafer K J and Krause J L 1993 Theoretical model for intense field high-order harmonic generation in rare gases *Laser Phys.* **3** 359–64
[8] Lein M, Hay N, Velotta R, Marangos J P and Knight P L 2002 Role of the intramolecular phase in high-harmonic generation *Phys. Rev. Lett.* **88** 183903–4
[9] Lein M, Hay N, Velotta R, Marangos J P and Knight P L 2002 Interference effects in high-order harmonic generation with molecules *Phys. Rev.* A **66** 023805–6
[10] Lein M, Corso P P, Marangos J P and Knight P L 2003 Orientation dependence of high-order harmonic generation in molecules *Phys. Rev.* A **67** 23819–1
[11] Lein M 2003 Antibonding molecular orbitals under the influence of elliptically polarized intense light *J. Phys. B: At. Mol. Opt. Phys.* **36** L155–61
[12] Kanai T, Minemoto S and Sakai H 2005 Quantum interference during high-order harmonic generation from aligned molecules *Nature* **435** 470–4
[13] Itatani J, Zeidler D, Levesque J, Spanner M, Villeneuve D M and Corkum P B 2005 Controlling high harmonic generation with molecular wave packets *Phys. Rev. Lett.* **94** 123902–4
[14] Vozzi C *et al* 2005 Controlling two-center interference in molecular high harmonic generation *Phys. Rev. Lett.* **95** 153902–4
[15] Vozzi C *et al* 2006 Probing two-centre interference in molecular high harmonic generation *J. Phys. B: At. Mol. Opt. Phys.* **39** S457–66
[16] Levesque J, Zeidler D, Marangos J P, Corkum P B and Villeneuve D M 2007 High harmonic generation and the role of atomic orbital wave functions *Phys. Rev. Lett.* **98** 183903
[17] Lewenstein M, Balcou Ph, Ivanov M Yu, L'Huillier A and Corkum P B 1994 Theory of high-harmonic generation by low-frequency laser fields *Phys. Rev.* A **49** 2117–32
[18] Frisch M J *et al* 2004 *Gaussian 03 Revision C.02* (Wallingford, CT: Gaussian Inc.)
[19] Smirnova O 2007 Private communication
[20] Zimmermann B, Lein M and Rost J M 2005 Analysis of recombination in high-order harmonic generation in molecules *Phys. Rev.* A **71** 033401
[21] Heritage J P, Gustafson T K and Lin C H 1975 Observation of coherent transient birefringence in CS_2 vapor *Phys. Rev. Lett.* **34** 1299–302
[22] Salières P, L'Huillier A and Lewenstein M 1995 Coherence control of high-order harmonics *Phys. Rev. Lett.* **74** 3776–9